

Experimentally identifying the entanglement class of pure tripartite states

Amandeep Singh,^{*} Kavita Dorai,[†] and Arvind[‡]

*Department of Physical Sciences, Indian Institute of Science Education & Research Mohali,
Sector 81 SAS Nagar, Manauli PO 140306 Punjab India.*

We use concurrence as an entanglement measure and experimentally demonstrate the entanglement classification of arbitrary three-qubit pure states on a nuclear magnetic resonance (NMR) quantum information processor. Computing the concurrence experimentally under three different bipartitions, for an arbitrary three qubit pure state, reveals the entanglement class of the state. The experiment involves measuring the expectation values of Pauli operators. This was achieved by mapping the desired expectation values onto the local z magnetization of a single qubit. We tested the entanglement classification protocol on twenty seven different generic states and successfully detected their entanglement class. Full quantum state tomography was performed to construct experimental tomographs of each state and negativity was calculated from them, to validate the experimental results.

PACS numbers: 03.67.Mn

I. INTRODUCTION

It is a well established fact that quantum entanglement is a key resource to achieve computational speedup in quantum information processing (QIP) tasks [1]. Entanglement characterization and detection is of utmost importance for the physical realization of quantum information processors [2, 3]. The presence of entanglement can be confirmed using several methods such as quantum state tomography [4], witness operators [5–7], the density operator under partial transposition [8, 9] and via the violation of Bell's inequalities [10].

Entangled states have been physically realized in superconducting phase qubits [11], nitrogen-vacancy defect centers [12], nuclear spin qubits [13], quantum dots [14] and trapped-ion [15] quantum computing hardware. Entanglement creation and detection has been demonstrated in NMR [16–20] and pseudo-bound entanglement was detected using a three-qubit system [21]. There are several measures to quantify and detect the entanglement [2, 22]. The entanglement of formation was used as an entanglement quantifier in four trapped ions [23], and concurrence [24] was measured in a single experiment on twin copies of the quantum state of photons [25]. Entanglement was also explored using witness based detection protocols in NMR [26] as well as in quantum optics [27].

The characterization and detection of multipartite entanglement is a challenging task in terms of the required experimental and computational resources [28–31]. It is hence important to design and experimentally implement entanglement detection protocols which use fewer resources. Three-qubit states have been classified into six inequivalent classes [36] under stochastic local operation and classical communication (SLOCC) [37] and several

protocols [32–35] have been proposed to ascertain the class of a given three state.

In the present study, we experimentally characterize the entanglement class of arbitrary three-qubit pure states. Towards achieving our goal we utilize a concurrence-based [24, 38] entanglement classification protocol proposed by Zhao et. al [33]. The advantage of this protocol is that it can be realized for any three-qubit pure state, as compared to previous proposals which are limited to the class of three-qubit generic states [39, 40]. The experimental implementation relies on efficiently determining the expectation values of desired Pauli operators and to achieve this we used a previously designed scheme which maps the expectation values onto the local z magnetization of a single qubit [41]. A total of twenty seven states were prepared to experimentally implement the protocol: seven representative states belonging to the six SLOCC inequivalent classes and twenty randomly generated states, with state fidelities ranging between 88% to 99%. The protocol successfully identified the entanglement class of all the seven representative states (namely, GHZ, W, $W\bar{W}$, three bi-separable states and a separable state) within the experimental error limits. Further, the randomly generated three-qubit states were also classified successfully as belonging to either the GHZ, the W, the bi-separable or the separable class of states. Full quantum state tomography [42] was performed and the entanglement measure negativity [43, 44] was computed from the experimentally reconstructed state, to validate the experimental results.

The paper is organized as follows: Section II outlines the theoretical framework for three-qubit entanglement classification where we describe the classification protocol. In Section III the NMR implementation of the protocol and our main results are described. Concluding remarks are contained in Section IV.

^{*} amandeepsingh@iisermohali.ac.in

[†] kavita@iisermohali.ac.in

[‡] arvind@iisermohali.ac.in

II. THREE QUBIT PURE STATE ENTANGLEMENT CLASSIFICATION

Consider a three-qubit pure state $|\Psi\rangle$. The state is fully separable if one can write $|\Psi\rangle = |\psi_1\rangle \otimes |\psi_2\rangle \otimes |\psi_3\rangle$. In case $|\Psi\rangle$ is biseparable under bipartition 1|23, then it is always possible to write $|\Psi\rangle = |\psi_1\rangle \otimes |\psi_{23}\rangle$ where the second and third qubits are in an entangled state $|\psi_{23}\rangle$. The other two possible bipartitions are 2|13 and 3|12. In case $|\Psi\rangle$ cannot be written as either a fully separable or a biseparable state, then the state is said to possess genuine tripartite entanglement. There are two SLOCC inequivalent classes of genuine three-qubit entanglement [36] namely, the GHZ and the W class. Hence any three-qubit pure state can belong to either of the six SLOCC inequivalent classes *i.e.* GHZ, W, three different bi-separable classes or the separable class of states [36].

We briefly outline below the procedure detailed in reference [33], for three-qubit pure state entanglement classification. The entanglement measure concurrence [24, 38] was used to identify biseparable states. The most general three-qubit pure state can be written as

$$|\Psi\rangle = \sum_{i,j,k=0}^1 a_{ijk} |ijk\rangle \quad \text{with} \quad \sum_{i,j,k=0}^1 |a_{ijk}|^2 = 1. \quad (1)$$

The concurrence for state $\rho = |\Psi\rangle\langle\Psi|$ in the 1|23 partition is given by $C(\rho) = \sqrt{1 - (\text{tr}\rho_1)^2}$ where $\rho_1 = \text{tr}_2(\rho)$ is the reduced density operator of the first party. The squared concurrence for a three-qubit pure state under the bipartition 1|23 is given by

$$C_{1|23}^2(\rho) = \sum_{j,k=0}^1 |a_{0jk}|^2 \cdot \sum_{j,k=0}^1 |a_{1jk}|^2 - \left| \sum_{j,k=0}^1 a_{0jk} a_{1jk}^* \right|^2 \quad (2)$$

After a lengthy calculation, it was shown in [33] that the squared concurrence (Eq. 2) can be written as a quadratic polynomial of the expectation values of Pauli operators for three qubits. Using the symbol $G_1(\rho)$ to denote $C_{1|23}^2(\rho)$, it takes the form

$$\begin{aligned} G_1(\rho) = & \frac{1}{16} (3 - \langle\sigma_0\sigma_0\sigma_3\rangle^2 - \langle\sigma_0\sigma_3\sigma_0\rangle^2 + \langle\sigma_3\sigma_3\sigma_0\rangle^2 \\ & - 3\langle\sigma_3\sigma_0\sigma_0\rangle^2 + \langle\sigma_3\sigma_0\sigma_3\rangle^2 - \langle\sigma_0\sigma_3\sigma_3\rangle^2 + \langle\sigma_3\sigma_3\sigma_3\rangle^2 \\ & - 3\langle\sigma_1\sigma_0\sigma_0\rangle^2 + \langle\sigma_1\sigma_0\sigma_3\rangle^2 + \langle\sigma_1\sigma_3\sigma_0\rangle^2 + \langle\sigma_1\sigma_3\sigma_3\rangle^2 \\ & - 3\langle\sigma_2\sigma_0\sigma_0\rangle^2 + \langle\sigma_2\sigma_0\sigma_3\rangle^2 + \langle\sigma_2\sigma_3\sigma_0\rangle^2 + \langle\sigma_2\sigma_3\sigma_3\rangle^2) \end{aligned} \quad (3)$$

with $\sigma_0 = |0\rangle\langle 0| + |1\rangle\langle 1|$, $\sigma_1 = |0\rangle\langle 1| + |1\rangle\langle 0|$, $\sigma_2 = i(|1\rangle\langle 0| - |0\rangle\langle 1|)$ and $\sigma_3 = |0\rangle\langle 0| - |1\rangle\langle 1|$ being Pauli matrices in the computational basis. Similar expressions for squared concurrences under the other two bipartitions *i.e.* $C_{2|13}^2(\rho)$ and $C_{3|12}^2(\rho)$ can be written by permutation and are symbolized by $G_2(\rho)$ and $G_3(\rho)$ respectively.

As described in *Theorem 1* of [33], for any three-qubit pure state $\rho = |\Psi\rangle\langle\Psi|$,

- (i) $|\Psi\rangle$ is fully separable iff $G_l(\rho) = 0$, for $l = 2, 3$ or $l = 1, 2$ or $l = 1, 3$.

- (ii) $|\Psi\rangle$ is separable between l^{th} qubit and rest iff $G_l(\rho) = 0$ and $G_m(\rho) > 0$ with $l, m \in \{1, 2, 3\}$ and $l \neq m$.

- (iii) $|\Psi\rangle$ is genuinely entangled iff $G_l(\rho) > 0$, for $l = 2, 3$ or $l = 1, 2$ or $l = 1, 3$.

Hence computing the entanglement witnesses $G_l(\rho)$, through experimentally measured expectation values of Pauli operators for an arbitrary three-qubit pure state $\rho = |\Psi\rangle\langle\Psi|$, can immediately reveal the entanglement class of the state.

As per *Theorem 1*-(iii) the current entanglement classification protocol enables us to decide if a given pure state has genuine three-qubit entanglement but does not specify if the state belongs to the GHZ or the W class. To overcome this limitation, we utilized our previous results [40] and define the observable $O = 2\sigma_1\sigma_1\sigma_1$ and use the n -tangle introduced in [47, 48] as an entanglement measure. For three qubits, a non-vanishing 3-tangle τ , implies the state belongs to the GHZ class. One may easily verify that for a given generic state $|\Psi\rangle$, the 3-tangle *i.e.* $\tau_\Psi = \langle\Psi|O|\Psi\rangle^2/4$. Having defined O in addition to $G_l(\rho)$, the protocol is now equipped to experimentally classify any three-qubit pure state.

A. Framework for Experimental Implementation

It has been established [46] that any three-qubit pure state can be transformed to a generic state of the canonical form

$$|\psi\rangle = a_0|000\rangle + a_1 e^{i\theta}|100\rangle + a_2|101\rangle + a_3|110\rangle + a_4|111\rangle \quad (4)$$

where $a_i \geq 0$, $\sum_i a_i^2 = 1$ and $\theta \in [0, \pi]$. It should be noted that the entanglement classification procedure outlined in Section II works for any three-qubit pure state but we chose to experimentally test it on arbitrary generic states, since different states may have the same generic canonical representation [46]. Entanglement properties for the class of all such states can be fully characterized resorting only to the SLOCC equivalent generic state representative of that class. Such a choice of states further eases the experimental implementation, as nearly 40% of the expectation values of the Pauli operators appearing in the expressions of $G_l(\rho)$ (*e.g.* Eq. 3) vanish in the case of generic states (Eq. 4). This entanglement classification protocol is not limited to generic states but also works for any arbitrary three-qubit pure state of form $|\Psi\rangle = \sum_{i,j,k=0}^1 a_{ijk} |ijk\rangle$.

B. Experimental Measurement of Observables using NMR

We use nuclear magnetic resonance (NMR) hardware to experimentally demonstrate the entanglement classification protocol. The crux of the detection protocol lies

in experimentally determining the expectation values of the observables appearing in Eq. 3. In order to experimentally find the expectation value of an observable it is a standard practice to decompose it as a linear superposition of some physically realizable basis operators. One such widely used operator basis is the Pauli basis [49, 50]. The next step is to map the desired basis operator expectation value to the experimentally accessible expectation value. In NMR the experimentally accessible information is the expectation value of Pauli z -operator for each qubit. We have previously developed and demonstrated such a mapping [40, 41] for any observable in NMR.

Assuming that we are interested in the expectation value of the operator O in the state $\rho = |\Psi\rangle\langle\Psi|$. To measure this we experimentally map the state $\rho \rightarrow \rho_i$ via map $\rho_i = U_i^\dagger \cdot \rho \cdot U_i$ followed by measuring the expectation value of Pauli z -operator in ρ_i . Explicit forms of U_i for two and three qubit systems are given in [41] and [40], respectively. It can be easily verified that $\langle O \rangle$ in ρ is equal to $\langle \sigma_3 \rangle$ in ρ_i with $U_i = \text{CNOT}_{23} \cdot \bar{Y}_3 \cdot \text{CNOT}_{12} \cdot \bar{Y}_2 \cdot \bar{Y}_1$. Here CNOT_{ij} is the controlled-NOT gate with i as the control qubit and j as the target qubit. $X(Y)$ are the local $\frac{\pi}{2}$ unitary rotation having phase $x(y)$. Bar over a phase represents negative phase. For the case of $\langle O \rangle$ in state ρ a quantum circuit to achieve the state mapping is shown in Fig. 1 (a).

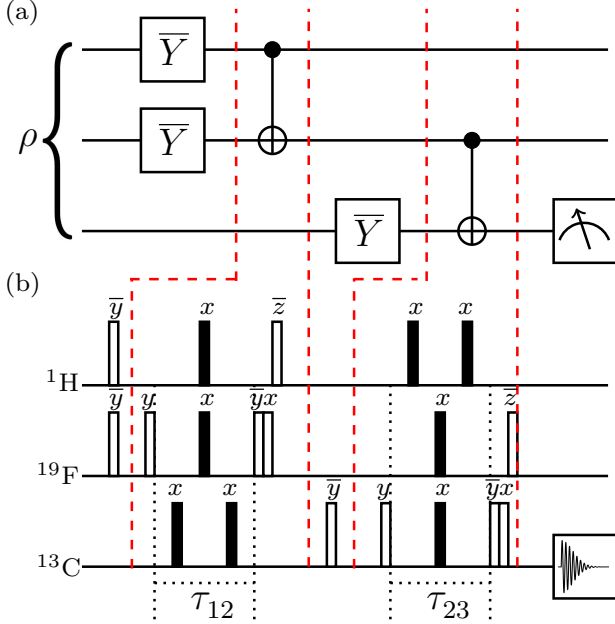


FIG. 1. (a) Quantum circuit to achieve mapping of the state ρ to ρ_i followed by measurement of qubit 3 in the computational basis. (b) NMR pulse sequence to implement the quantum circuit given in (a). The unfilled rectangles denote $\frac{\pi}{2}$ spin-selective RF pulses while the filled rectangles denote π pulses. Pulse phases are written above the respective pulse and a bar over a phase represents negative phase. Delays are given by $\tau_{ij} = 1/(8J_{ij})$; i, j label the qubit and J denotes the scalar coupling constant.

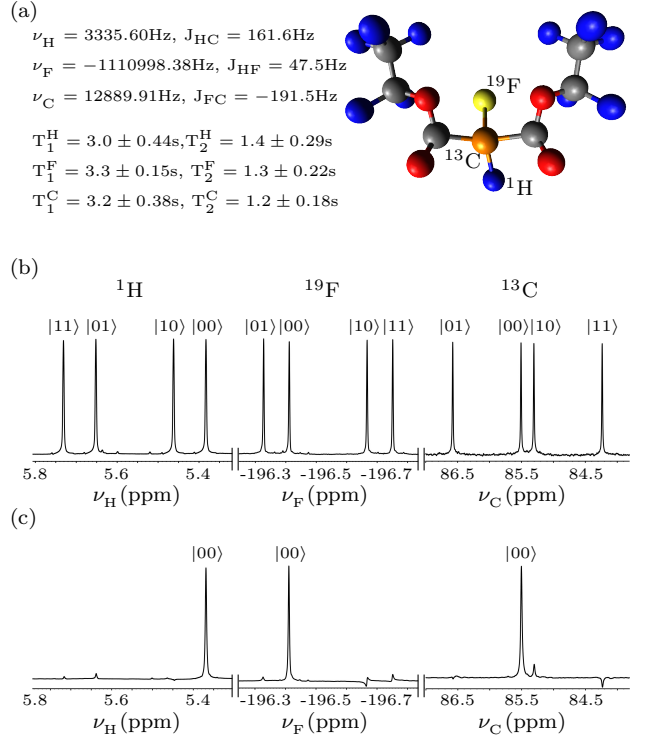


FIG. 2. (a) Molecular structure of ^{13}C -labeled diethyl fluoromalonate and NMR parameters. NMR spectra of (b) thermal equilibrium state and (c) pseudopure state. Each peak is labeled with the logical state of the passive qubit during the transition.

III. NMR IMPLEMENTATION OF THREE QUBIT ENTANGLEMENT CLASSIFICATION PROTOCOL

The Hamiltonian [51] in frequency units, for three qubits in the rotating frame can be written as

$$\mathcal{H} = - \sum_{i=1}^3 \nu_i I_{iz} + \sum_{i>j, i=1}^3 J_{ij} I_{iz} I_{jz} \quad (5)$$

where the indices $i, j = 1, 2$ or 3 are the qubit labels, ν_i is the chemical shift, J_{ij} is the scalar coupling constant, and I_{iz} is the z -spin angular momentum operator of the i^{th} spin.

For the experimental implementation of the entanglement classification protocol, ^{13}C labeled diethylfluoromalonate dissolved in acetone- D_6 sample was used, with the ^1H , ^{19}F and ^{13}C nuclei serving as qubit 1, qubit 2 and qubit 3, respectively. Before preparing arbitrary three-qubit pure states, the system was initialized in the pseudopure (PPS) state $|000\rangle$ utilizing spatial averaging [52] with the PPS density operator given by

$$\rho_{000} = \frac{1-\epsilon}{2^3} \mathbb{I}_8 + \epsilon |000\rangle\langle 000| \quad (6)$$

where $\epsilon \sim 10^{-5}$ is the thermal magnetic polarization at room temperature and \mathbb{I}_8 is the 8×8 identity opera-

tor. The experimental NMR parameters (rotating frame chemical shifts, T_1 and T_2 relaxation times and scalar couplings J_{ij}) as well as the NMR spectra of the thermal equilibrium and PPS states are shown in Fig. 2. Each spectral transition in the NMR spectrum is labeled with the logical states of the passive qubits (*i.e.* qubits not undergoing any transition) in the computational basis. Experimentally prepared PPS had fidelity (Fig. 2(c)) 0.98 ± 0.01 and was computed using the fidelity measure [54, 55]

$$F = \left[\text{Tr} \left(\sqrt{\sqrt{\rho_{th}} \rho_{ex} \sqrt{\rho_{th}}} \right) \right]^2 \quad (7)$$

where ρ_{th} and ρ_{ex} are the theoretically expected and the experimentally reconstructed density operators, respectively. Fidelity measure is normalized in the sense that $F \rightarrow 1$ as $\rho_{ex} \rightarrow \rho_{th}$. Experimental reconstruction of the density operator was achieved via full quantum state tomography (QST)[42, 56] utilizing a preparatory pulse set of $\{III, XXX, IYY, XYX, YII, XXY, IYY\}$, where I implies “no operation”. In NMR a $\frac{\pi}{2}$ local unitary rotation $X(Y)$ can be achieved using highly accurate and calibrated spin-selective transverse radio frequency (RF) pulses having phase $x(y)$.

A Bruker Avance-III 600-MHz FT-NMR spectrometer equipped with a QXI probe was used for the experiments which were performed at room temperature (293K). A spin specific pulse calibration yields the duration, amplitude and phase to achieve the desired local unitary operation. Free evolution under the Hamiltonian Eq. 5 for a desired duration was used to achieve non-local unitary operations. $\frac{\pi}{2}$ spin selective pulses for ^1H , ^{19}F and ^{13}C in the current study were $9.40 \mu\text{s}$ at 18.14 W power level, $22.50 \mu\text{s}$ at a power level of 42.27 W and $16.00 \mu\text{s}$ at a power level of 179.47 W, respectively.

For the experimental demonstration of the entanglement classification protocol discussed in Section II, we prepared the three qubits in twenty seven different states. Seven states were prepared from the six SLOCC inequivalent entanglement classes *i.e.* GHZ (GHZ and $\overline{\text{WW}}$ states), W, three bi-separable and from the separable class of states. We labeled three biseparable class states under partitions 1|23, 2|13 and 3|12 as BS_1 , BS_2 and BS_3 respectively. Additionally, twenty random generic states were prepared using a random number generator and labeled as R_1 , R_2 , R_3 ,....., R_{20} . The details of the quantum circuits as well as NMR pulse sequences required to prepare all the desired quantum states in the current study are given in Reference [13]. All the prepared states were found to have the fidelity (F) in the range 0.88 to 0.99. For each prepared state the expectation values of the Pauli operators were determined as described in Section IIB which in turn was used to compute $G_l(\rho)$ using Eq. 3. $\langle O \rangle$ was also found in all the cases as it serves as an entanglement witness of the GHZ class.

Experimental results of the three-qubit entanglement classification and detection protocol are shown in Table I.

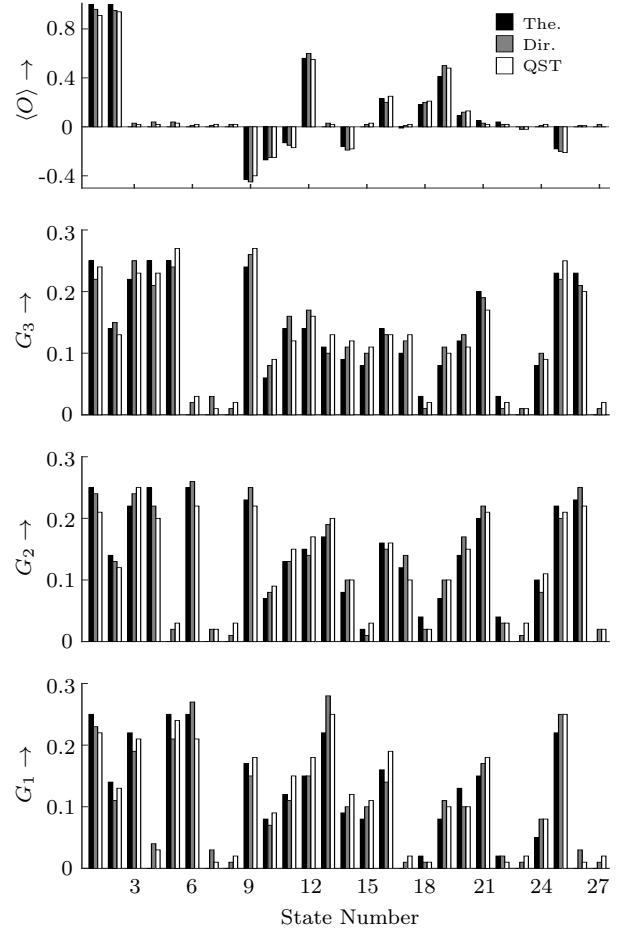


FIG. 3. Bar plots of the expectation value of the observable O and the squared concurrences G_1 , G_2 and G_3 for states numbered from 1-27 (Table I). The state number is represented on the horizontal axes while the values of the respective observable are represented along the vertical axes. Black, gray and unfilled bars represent the theoretical (The.) values, directly experimentally measured values (Dir.), and QST-derived values, respectively.

A bar chart has been plotted in Fig. 3 for a visual representation of the experimental results of Table I. To obtain the bar plots of Fig. 3, the experimentally prepared states were numbered from 1 to 27 as per the ordering in Table I. As detailed in Sec. II, the concurrence $G_l(\rho)$ acts as an entanglement witness, and the additional observable O helps in the experimental discrimination of GHZ class states from the rest. In order to validate the experimental results we also computed the negativity [43, 44] from the experimentally reconstructed state via QST [42] and the results are shown in Table II. In each case, the experiments were repeated several times for experimental error estimates. Experimental errors were in the range of 2.2% - 5.7% for the values reported in the Table I.

As observed from Table I, the seven states, from six SLOCC inequivalent classes, were prepared with experimental fidelity ≥ 0.95 . The entanglement classes of all these seven states were correctly identified with the cur-

TABLE I. Results of entanglement classification protocol for twenty seven states. Label BS denotes a biseparable state while R denotes a randomly prepared state. The first column depicts the state label, the top row lists the observable (Obs.) while the second row specifies if the observable value obtained is theoretical (The.), from QST or direct experimentally determined (Dir.).

Obs. → State (F) ↓	$\langle O \rangle$			G_1			G_2			G_3		
	The.	QST	Dir.	The.	QST	Dir.	The.	QST	Dir.	The.	QST	Dir.
GHZ(0.96±0.01)	1.00	0.96	0.91	0.25	0.23	0.22	0.25	0.24	0.21	0.25	0.22	0.24
WW(0.95±0.02)	1.00	0.95	0.94	0.14	0.11	0.13	0.14	0.13	0.12	0.14	0.15	0.13
W(0.96±0.02)	0	0.03	0.02	0.22	0.19	0.21	0.22	0.24	0.25	0.22	0.25	0.23
BS ₁ (0.98±0.01)	0	0.04	0.02	0	0.04	0.03	0.25	0.22	0.20	0.25	0.21	0.23
BS ₂ (0.94±0.03)	0	0.04	0.03	0.25	0.21	0.24	0	0.02	0.03	0.25	0.24	0.27
BS ₃ (0.95±0.02)	0	0.01	0.02	0.25	0.27	0.21	0.25	0.26	0.22	0	0.02	0.03
Sep(0.98±0.01)	0	0.01	0.02	0	0.03	0.01	0	0.02	0.02	0	0.03	0.01
R ₁ (0.92±0.03)	0	0.02	0.02	0	0.01	0.02	0	0.01	0.03	0	0.01	0.02
R ₂ (0.93±0.02)	-0.43	-0.45	-0.40	0.17	0.15	0.18	0.23	0.25	0.22	0.24	0.26	0.27
R ₃ (0.96±0.02)	-0.27	-0.25	-0.25	0.08	0.07	0.09	0.07	0.08	0.09	0.06	0.08	0.09
R ₄ (0.94±0.03)	-0.13	-0.15	-0.17	0.12	0.11	0.15	0.13	0.13	0.15	0.14	0.16	0.12
R ₅ (0.93±0.02)	0.56	0.60	0.55	0.15	0.15	0.18	0.15	0.14	0.17	0.14	0.17	0.16
R ₆ (0.89±0.01)	0	0.03	0.02	0.22	0.28	0.25	0.17	0.19	0.20	0.11	0.10	0.13
R ₇ (0.96±0.02)	-0.16	-0.19	-0.18	0.09	0.10	0.12	0.08	0.10	0.10	0.09	0.11	0.12
R ₈ (0.93±0.02)	0	0.02	0.03	0.08	0.10	0.11	0.02	0.01	0.03	0.08	0.10	0.11
R ₉ (0.97±0.03)	0.23	0.20	0.25	0.16	0.14	0.19	0.16	0.15	0.16	0.14	0.13	0.13
R ₁₀ (0.93±0.02)	-0.01	0.01	0.02	0	0.01	0.02	0.12	0.14	0.10	0.10	0.12	0.13
R ₁₁ (0.94±0.01)	0.18	0.20	0.21	0.02	0.01	0.01	0.04	0.02	0.02	0.03	0.01	0.02
R ₁₂ (0.95±0.02)	0.41	0.50	0.48	0.08	0.11	0.10	0.07	0.10	0.10	0.08	0.11	0.10
R ₁₃ (0.93±0.01)	0.09	0.12	0.13	0.13	0.10	0.10	0.14	0.17	0.15	0.12	0.13	0.11
R ₁₄ (0.94±0.02)	0.05	0.03	0.02	0.15	0.17	0.18	0.20	0.22	0.21	0.20	0.19	0.17
R ₁₅ (0.98±0.01)	0.04	0.02	0.02	0.02	0.02	0.01	0.04	0.03	0.03	0.03	0.01	0.02
R ₁₆ (0.96±0.01)	0	-0.02	-0.02	0	0.01	0.02	0	0.01	0.03	0	0.01	0.01
R ₁₇ (0.95±0.02)	0	0.01	0.02	0.05	0.08	0.08	0.10	0.08	0.11	0.08	0.10	0.09
R ₁₈ (0.90±0.02)	-0.18	-0.20	-0.21	0.22	0.25	0.25	0.22	0.20	0.21	0.23	0.22	0.25
R ₁₉ (0.94±0.02)	0	0.01	0.01	0	0.03	0.01	0.23	0.25	0.22	0.23	0.21	0.20
R ₂₀ (0.96±0.02)	0	0.02	0	0	0.01	0.02	0	0.02	0.02	0	0.01	0.02

rent protocol. Further, the states R₂, R₃, R₄, R₅, R₆, R₇, R₈, R₉, R₁₁, R₁₂, R₁₃, R₁₄, R₁₇ and R₁₈ have at least two non-zero concurrences and hence are genuinely entangled states. This fact is further supported by negativity of these states as reported in Table II. As discussed earlier, in order to discriminate GHZ class from the rest one can resort to the observable O . Non vanishing values of $\langle O \rangle$ in Table I imply that the states R₂, R₃, R₄, R₅, R₇, R₉, R₁₁, R₁₂, R₁₃ and R₁₈ belong to the GHZ class. In contrast, the genuinely entangled states R₆, R₈, R₁₄ and R₁₇ have vanishing values of $\langle O \rangle$ and hence have vanishing 3-tangle as well, so they were identified as belonging to the W class. States R₁₀ and R₁₉ have vanishing concurrence G_1 implying that these states belong to BS₁ class. Also states R₁, R₁₅, R₁₆ and R₂₀ were identified as separable as all the observables have near zero values as well as zero negativity.

IV. CONCLUDING REMARKS

We experimentally classified the entanglement of arbitrary three-qubit pure states using the concurrence as an entanglement measure. Concurrence was measured experimentally by measuring the expectation values of the Pauli operators under all three bipartitions. To demonstrate the efficacy of the entanglement classification scheme experimentally, we tested the protocol on seven standard as well as twenty random three-qubit pure states prepared on an NMR quantum information processor. The entanglement class of all the seven states representing six SLOCC classes was correctly identified. The results were validated using full QST and negativity calculations for each state. The entanglement class of the twenty random states was also identified within experimental error limits. Non-zero negativity as well as two out of three concurrence witnesses indicated that the

TABLE II. Theoretically calculated and experimentally measured negativity values for all twenty seven states under investigation.

Negativity \rightarrow State \downarrow	Theoretical	Experimental
GHZ	0.5	0.47 ± 0.02
WW	0.37	0.39 ± 0.02
W	0.47	0.44 ± 0.01
BS ₁	0	0.02 ± 0.02
BS ₂	0	0.03 ± 0.01
BS ₃	0	0.02 ± 0.02
Sep	0	0.02 ± 0.02
R ₁	0	0.01 ± 0.01
R ₂	0.46	0.43 ± 0.04
R ₃	0.26	0.24 ± 0.03
R ₄	0.18	0.17 ± 0.03
R ₅	0.38	0.35 ± 0.02
R ₆	0.40	0.37 ± 0.04
R ₇	0.29	0.31 ± 0.03
R ₈	0.22	0.21 ± 0.02
R ₉	0.39	0.37 ± 0.04
R ₁₀	0.03	0.01 ± 0.01
R ₁₁	0.17	0.14 ± 0.02
R ₁₂	0.27	0.30 ± 0.03
R ₁₃	0.16	0.12 ± 0.04
R ₁₄	0.42	0.37 ± 0.04
R ₁₅	0.02	0.03 ± 0.01
R ₁₆	0	0.01 ± 0.01
R ₁₇	0.26	0.22 ± 0.03
R ₁₈	0.47	0.41 ± 0.04
R ₁₉	0	0.02 ± 0.02
R ₂₀	0	0.03 ± 0.02

state under investigation had genuine three-qubit entanglement. Such states may belong to either the GHZ or the W class. To further differentiate the entanglement class, we measured the three-tangle in each case, since non-zero three-tangle is a signature of the GHZ class. Based on this, the experimental classification protocol successfully classified randomly generated states as belonging to either the GHZ class or W class of entangled states or as biseparable or separable states. Future directions of this work include evaluating the performance of the protocol for mixed states as well as for larger qubit registers.

ACKNOWLEDGMENTS

All the experiments were performed on a Bruker Avance-III 600 MHz FT-NMR spectrometer at the NMR Research Facility of IISER Mohali. Arvind acknowledges funding from DST India under Grant No. EMR/2014/000297. K.D. acknowledges funding from DST India under Grant No. EMR/2015/000556.

-
- [1] R. Horodecki, P. Horodecki, M. Horodecki, and K. Horodecki, *Rev. Mod. Phys.*, **81**, 865 (2009).
 - [2] O. Gühne and G. Tóth, *Phys. Rep.*, **474**, 1 (2009).
 - [3] M. Li, M.-J. Zhao, S.-M. Fei, and Z.-X. Wang, *Front. Phys.*, **8**, 357 (2013).
 - [4] R. T. Thew, K. Nemoto, A. G. White, and W. J. Munro, *Phys. Rev. A*, **66**, 012303 (2002).
 - [5] O. Gühne, P. Hyllus, D. Bruß, A. Ekert, M. Lewenstein, C. Macchiavello, and A. Sanpera, *J. Mod. Optics*, **50**, 1079 (2003).
 - [6] J. M. Arrazola, O. Gittsovich, and N. Lütkenhaus, *Phys. Rev. A*, **85**, 062327 (2012).
 - [7] B. Junnitsch, T. Moroder, and O. Gühne, *Phys. Rev. Lett.*, **106**, 190502 (2011).
 - [8] A. Peres, *Phys. Rev. Lett.*, **77**, 1413 (1996).
 - [9] M. Li, J. Wang, S. Shen, Z. Chen, and S.-M. Fei, *Sci. Rep.*, **7**, 17274 (2017).
 - [10] D. P. DiVincenzo and A. Peres, *Phys. Rev. A*, **55**, 4089 (1997).
 - [11] M. Neeley, R. C. Bialczak, M. Lenander, E. Lucero, M. Mariantoni, A. D. O'Connell, D. Sank, H. Wang, M. Weides, J. Wenner, Y. Yin, T. Yamamoto, A. N. Cleland, and J. M. Martinis, *Nature*, **467**, 570 (2010).
 - [12] P. Neumann, N. Mizuochi, F. Rempp, P. Hemmer, H. Watanabe, S. Yamasaki, V. Jacques, T. Gaebel, F. Jelezko, and J. Wrachtrup, *Science*, **320**, 1326 (2008).
 - [13] S. Dogra, K. Dorai, and Arvind, *Phys. Rev. A*, **91**, 022312 (2015).
 - [14] W. B. Gao, P. Fallahi, E. Togan, J. Miguel-Sanchez, and A. Imamoglu, *Nature*, **491**, 426 (2012).
 - [15] O. Mandel, M. Greiner, A. Widera, T. Rom, T. W. Hänsch, and I. Bloch, *Nature*, **425**, 937 (2003).
 - [16] R. Laflamme, E. Knill, W. H. Zurek, P. Catasti, and S. Mariappan, *Philos. Trans. R. Soc. London, Ser A*, **356**, 1941 (1998).
 - [17] X. Peng, J. Zhang, J. Du, and D. Suter, *Phys. Rev. A*, **81**, 042327 (2010).

- [18] K. R. K. Rao and A. Kumar, *Int. J. Quantum Info.*, **10**, 1250039 (2012).
- [19] D. Das, S. Dogra, K. Dorai, and Arvind, *Phys. Rev. A*, **92**, 022307 (2015).
- [20] T. Xin, J. S. Pedernales, E. Solano, and G.-L. Long, *Phys. Rev. A*, **97**, 022322 (2018).
- [21] H. Kampermann, D. Bruß, X. Peng, and D. Suter, *Phys. Rev. A*, **81**, 040304 (2010).
- [22] D. Bruß, *J. Math. Phys.*, **43**, 4237 (2002).
- [23] C. A. Sackett, D. Kielpinski, B. E. King, C. Langer, V. Meyer, C. J. Myatt, M. Rowe, Q. A. Turchette, W. M. Itano, D. J. Wineland, and C. Monroe, *Nature*, **404**, 256 (2000).
- [24] W. K. Wootters, *Quantum Info. Comput.*, **1**, 27 (2001).
- [25] S. P. Walborn, P. H. Souto Ribeiro, L. Davidovich, F. Mintert, and A. Buchleitner, *Nature*, **440**, 1022 (2006).
- [26] J. G. Filgueiras, T. O. Maciel, R. E. Auccaise, R. O. Vianna, R. S. Sarthour, and I. S. Oliveira, *Quant. Inf. Proc.*, **11**, 1883 (2012).
- [27] M. Bourennane, M. Eibl, C. Kurtsiefer, S. Gaertner, H. Weinfurter, O. Gühne, P. Hyllus, D. Bruß, M. Lewenstein, and A. Sanpera, *Phys. Rev. Lett.*, **92**, 087902 (2004).
- [28] W. Dür and J. I. Cirac, *J. Phys. A: Math. Gen.*, **34**, 6837 (2001).
- [29] J. B. Altepeter, E. R. Jeffrey, P. G. Kwiat, S. Tanzilli, N. Gisin, and A. Acín, *Phys. Rev. Lett.*, **95**, 033601 (2005).
- [30] C. Spengler, M. Huber, S. Brierley, T. Adaktylos, and B. C. Hiesmayr, *Phys. Rev. A*, **86**, 022311 (2012).
- [31] J. Dai, Y. L. Len, Y. S. Teo, B.-G. Englert, and L. A. Krivitsky, *Phys. Rev. Lett.*, **113**, 170402 (2014).
- [32] D. P. Chi, K. Jeong, T. Kim, K. Lee, and S. Lee, *Phys. Rev. A*, **81**, 044302 (2010).
- [33] M.-J. Zhao, T.-G. Zhang, X. Li-Jost, and S.-M. Fei, *Phys. Rev. A*, **87**, 012316 (2013).
- [34] Y. Akbari-Kourbolagh, *Int. J. Quant. Inf.*, **15**, 1750049 (2017).
- [35] Y. Akbari-Kourbolagh and M. Azhdargalam, *Phys. Rev. A*, **97**, 042333 (2018).
- [36] W. Dür, G. Vidal, and J. I. Cirac, *Phys. Rev. A*, **62**, 062314 (2000).
- [37] C. H. Bennett, S. Popescu, D. Rohrlich, J. A. Smolin, and A. V. Thapliyal, *Phys. Rev. A*, **63**, 012307 (2000).
- [38] W. K. Wootters, *Phys. Rev. Lett.*, **80**, 2245 (1998).
- [39] S. Adhikari, C. Datta, A. Das, and P. Agrawal, *arXiv* (2017), 1705.01377.
- [40] A. Singh, H. Singh, K. Dorai, and Arvind, *arXiv* (2018), 1804.09320.
- [41] A. Singh, Arvind, and K. Dorai, *Phys. Rev. A*, **94**, 062309 (2016).
- [42] G. M. Leskowitz and L. J. Mueller, *Phys. Rev. A*, **69**, 052302 (2004).
- [43] Y. S. Weinstein, *Phys. Rev. A*, **82**, 032326 (2010).
- [44] G. Vidal and R. F. Werner, *Phys. Rev. A*, **65**, 032314 (2002).
- [45] P. Rungta, V. Bužek, C. M. Caves, M. Hillery, and G. J. Milburn, *Phys. Rev. A*, **64**, 042315 (2001).
- [46] A. Acín, D. Bruß, M. Lewenstein, and A. Sanpera, *Phys. Rev. Lett.*, **87**, 040401 (2001).
- [47] A. Wong and N. Christensen, *Phys. Rev. A*, **63**, 044301 (2001).
- [48] D. Li, *Quant. Inf. Proc.*, **11**, 481 (2012), ISSN 1573-1332.
- [49] M. A. Nielsen and I. L. Chuang, *Quantum Computation and Quantum Information* (Cambridge University Press, 2000) ISBN 0511976666.
- [50] I. S. Oliveira, T. J. Bonagamba, R. S. Sarthour, J. C. C. Freitas, and E. R. deAzevedo, *NMR Quantum Information Processing* (Elsevier, Linacre House, Jordan Hill, Oxford OX2 8DP, UK, 2007).
- [51] R. R. Ernst, G. Bodenhausen, and A. Wokaun, *Principles of NMR in One and Two Dimensions* (Clarendon Press, 1990) ISBN 0198556470.
- [52] D. G. Cory, M. D. Price, and T. F. Havel, *Physica D: Nonlinear Phenomena*, **120**, 82 (1998).
- [53] A. Mitra, K. Sivapriya, and A. Kumar, *J. Magn. Reson.*, **187**, 306 (2007).
- [54] A. Uhlmann, *Rep. Math. Phys.*, **9**, 273 (1976).
- [55] R. Jozsa, *J. Mod. Optics*, **41**, 2315 (1994).
- [56] H. Singh, Arvind, and K. Dorai, *Physics Letters A*, **380**, 3051 (2016).